Primary Folding Dynamics of Sperm Whale Apomyoglobin: Core Formation

Miriam Gulotta,* Eduard Rogatsky,* Robert H. Callender,* and R. Brian Dyer†
*Department of Biochemistry, Albert Einstein College of Medicine, Bronx, New York 10461; and
†Bioscience Division, Mail Stop J586, Los Alamos National Laboratory, Los Alamos, New Mexico 87545

ABSTRACT The structure, thermodynamics, and kinetics of heat-induced unfolding of sperm whale apomyoglobin core formation have been studied. The most rudimentary core is formed at pH* 3.0 and up to 60 mM NaCl. Steady state for ultraviolet circular dichroism and fluorescence melting studies indicate that the core in this acid-destabilized state consists of a heterogeneous composition of structures of ~26 residues, two-thirds of the number involved for horse heart apomyoglobin under these conditions. Fluorescence temperature-jump relaxation studies show that there is only one process involved in Trp burial. This occurs in 20 μs for a 7° jump to 52°C, which is close to the limits placed by diffusion on folding reactions. However, infrared temperature jump studies monitoring native helix burial are biexponential with times of 5 μs and 56 μs for a similar temperature jump. Both fluorescence and infrared fast phases are energetically favorable but the slow infrared absorbance phase is highly temperature-dependent, indicating a substantial enthalpic barrier for this process. The kinetics are best understood by a multiple-pathway kinetics model. The rapid phases likely represent direct burial of one or both of the Trp residues and parts of the G- and H-helices. We attribute the slow phase to burial and subsequent rearrangement of a misformed core or to a collapse having a high energy barrier wherein both Trps are solvent-exposed.

INTRODUCTION

Myoglobin (Mb) is a relatively simple, single-domain globular protein composed of 153 amino acids, with no disulfide bonds and no other secondary structure apart from eight α-helices, labeled A–H, and the turns which connect them. Despite this simplicity, it does not fold via two-state kinetics, but rather is one of a class of proteins that fold through an intermediate having a single central compact hydrophobic core consisting of ~55 residues at the intersection of the A-helix with the G- and H-helices and the G-H hairpin. The holoprotein is very stable, but once its heme has been removed to form apomyoglobin (apoMb), it is easily unfolded and several partially folded states can be populated at equilibrium by adjusting pH, salt concentration, and temperature. The native, N, and the various acid-denatured forms of apomyoglobin (I, E, and U—obtained by progressively lower pH) have been characterized thermodynamically and kinetically (Griko et al., 1988; Hughson et al., 1990; Griko and Privalov, 1994; Loh et al., 1995; Eliezer and Wright, 1996; Lecomte et al., 1996; Gilmanshin et al., 1997; Jamin and Baldwin, 1998). Both the I-form at pH 4 as well as the unfolded U-form at pH 2.3 (minimal salt) of sperm whale apomyoglobin were recently investigated by NMR (Dyson and Wright, 1998; Eliezer et al., 1998, 2000; Yao et al., 2001).

Our laboratory has studied the structure of E in the horse heart protein, formed at pH 3.0 and 20–30 mM NaCl and believed to be the most acid-destabilized form still containing some compact structure, by fluorescence, for ultraviolet (UV) circular dichroism (CD), and infrared absorbance (IR) absorption (Gilmanshin et al., 1997; Gilmanshin et al., 2001), and its folding kinetics determined by both fluorescence and infrared temperature-jump relaxation spectroscopy (Gilmanshin et al., 1998; Gulotta et al., 2001). It was found that the folded structure of horse heart E contains a diminished portion of the A-G-H core (30–40 residues) with no other tertiary structure and probably little other secondary structure apart from that in the core. E melts to U with fairly steep melting curves whose shapes, however, depend on the specific spectroscopic probe used to monitor melting. The relaxation kinetics of core formation in the E to U interconversion were found to be multiple-exponential, or at least biexponential, and fast, on the microsecond time scale. Overall, we found that the formation of E from the unfolded state is best described by a multiple-pathway kinetic model when U collapses to form not a single shape for folded E but an ensemble of folded core structures.

The goal of this work is to characterize the E-form of sperm whale apomyoglobin, both its static structure and its formation kinetics, and compare these results to those found for E of horse heart apomyoglobin. Most previous structural and dynamics studies of apoMb concern the sperm whale protein. In addition, the two proteins have somewhat different primary sequences and stabilities, which make them interesting for comparison. Static probes of structure include: Trp fluorescence, IR, and CD spectroscopies. Kinetic characterization of folding/unfolding is accomplished using laser-induced temperature-jump (T-jump) to initiate unfolding dynamics on the nanosecond time scale, and using both IR absorption in the structurally sensitive amide-I′ absorption band and Trp fluorescence emission to monitor structural changes.

Submitted April 2, 2002, and accepted for publication November 6, 2002.
Address reprint requests to Miriam Gulotta, Tel.: 718-430-2437; Fax: 718-430-8565; E-mail: gulotta@aecom.yu.edu.

0006-3495/03/03/1909/10 $2.00

MATERIALS AND METHODS

Materials

The plasmid for wild-type sperm whale myoglobin was a gift of Dr. Stephen Sligar. Its preparation has been described in detail by his laboratory (Springer and Sligar, 1987). For our purposes, the plasmid was grown in BL 21 de3 electrocompetent *Escherichia coli* cells. The cells were lysed using a French press (10,000 psi) followed by sonication. The resulting solution was then heated to 52°C for 30 min. The debris was spun down and discarded. The blood red supernatant was loaded onto a Ni-His bind-NTA column (Novagen, Madison, WI) (1.6 × 25 cm) previously equilibrated in 0.03 M Tris, 1M NaCl, pH 7.4 buffer. Mb was eluted using 0.03 M Tris, pH 8.8 buffer. The eluted Mb was concentrated to 20 ml or less and loaded onto a DEAE-FF Sepharose column (2.5 × 20 cm). The eluted Mb was heated to 65°C for 10 min. Any precipitated protein was removed by centrifugation. If the Soret/protein ratio was low, the supernatant was reloaded on the nickel column and eluted as above. The final protein solution was stored at 4°C. Before extraction, the excess salt and the Tris were removed either by dialysis against distilled water or by washing using an Amicon-stirred cell. The Mb was then concentrated down and glycine added to 0.1 M. For the extraction, the Mb/glycine solution was put on ice and gently stirred. The pH was dropped to 1 using 1 N HCl, and the heme was immediately extracted out using 2-butanone. The 2-butanone was removed by dialysis, and the protein solution was loaded onto a G-75 column to remove any aggregates. Extensive dialysis against distilled water was used to remove as much residual salt as possible. The pure apomyoglobin was then lyophilized to dryness and stored at −70°C. UV absorbance was used to check the purity of the product; only apomyoglobin samples having less than 1% heme remaining were used.

A stock apomyoglobin solution was prepared by first dissolving the lyophilized apomyoglobin in the appropriate solvent, and then adjusting the pH* accordingly using a minimal amount of DCl. The pH* is the uncorrected (for D_2O) pH-meter reading at room temperature. Lyophilized protein always includes residual salt and water. As the apoMb structure at low pH* is extremely sensitive to the actual salt concentration, gel filtration on a Sephadex G25 column was performed to remove any excess salt as well as separate out any aggregates from the protein solution. For Fourier Transform Infrared (FTIR) spectroscopy, the buffer fraction immediately preceding the protein peak was collected and used as a reference to ensure the precise balance of residual HOD. The collected protein solution was isolated as it left the column. Aliquots of the eluted fractions were used to determine protein concentration ($E^{1\%}_{280} = 0.93$; Crumpton and Polson, 1965).

To determine the conditions for the formation of E-form sperm whale apomyoglobin, the fluorescence spectrum was taken as a function of chloride ion concentration. Fig. 1 shows the dependence of fluorescence emission λ_{max} as a function of anion concentration. There is clearly a break point in the curve at low anion concentration (less than 60 mM for the sperm whale protein) which is similar to that found for horse heart apomyoglobin (Gilmanshin et al., 2001). Therefore, the conditions used in preparing E-form sperm whale apomyoglobin were taken to be the same as those used for preparing apomyoglobin from horse heart.

The reversibility of the temperature denaturation was checked by scanning upward to a specific high temperature and then cooling. Reversibility was within 10% for all of the data presented herein.

Fluorescence measurements

Fluorescence spectra were recorded on a FluoroMax-2 spectrofluorimeter (Instruments S.A., Edison, NJ) with correction for a spectral dependence of registration response. The excitation wavelength was 290 nm. Similar results were obtained using 275-nm excitation. A 3-nm bandpass was used for both excitation and emission. Samples with concentrations of 0.05 mg/mL in a 1-cm^2 fused silica cuvette were used. The data were collected and processed with the DataMax software (Instruments S.A.).

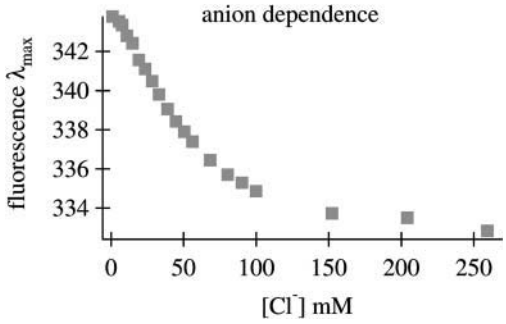

FIGURE 1 Plot of fluorescence emission λ_{max} as a function of [Cl^-] for sperm whale apomyoglobin at pH* 3.0.

Infrared spectroscopy

Static infrared spectra were obtained using a Nicolet 760 FTIR spectrometer (ThermoNicolet, Madison, WI). Sample concentrations of 2–4 mg/ml were used for the IR measurements. A CaF_2 cell with a Teflon spacer of 50 μm was used for the equilibrium measurements. No aggregation was observed (marker amide I-bands indicative of aggregation are readily observed) in equilibrium measurements at concentrations of <5 mg/mL. All spectra shown at a specific temperature are constructed by subtracting the spectrum of buffer solution without protein from solution with protein; this is done because the buffer water exhibits a temperature-dependent IR spectrum (Williams et al., 1996). Temperature-dependent difference spectra were then created by subtracting the so-obtained spectrum at 11°C from the spectrum at the temperature listed. The second derivatives were smoothed with a fourth-order, 19-point Savitzky-Golay algorithm (which corresponds to ~20-cm^{-1} bandpass filter).

CD spectroscopy

CD spectra were taken on a Jasco J-720 spectrometer (Jasco, Easton, MD) equipped with a temperature-controlled cuvette holder. The spectrometer was calibrated using *d*-camphorsulfonic acid. Rectangular 1-mm pathlength quartz cuvettes were used for the measurements. Each spectrum is an average of two scans taken between 260 and 190 nm at either 50 or 100 nm/min. The sensitivity setting was 20 mdeg, and the response time was 1 s. The slit width was set at 1.0 mm which gave a 0.5-nm resolution. The data were analyzed by subtracting any background CD spectrum and converting the spectra from millidegrees to molar ellipticity ([Θ]) in degrees per square centimeter per decimole residues. A stock protein solution with a known concentration was added to a solution of the same solvent to make a final solution with a concentration between 0.01 and 0.02 mg/mL. The final solution was then scanned in the UV spectrometer to ensure that the absorbance below 200 nm was not greater than 1.

Temperature-jump spectrometers

The essence of the kinetics spectrometer is the same for the IR and fluorescence temperature-jump instruments. A continuous laser beam, whose wavelength lies either in the IR within the structurally sensitive amide-I′ protein band or at 275 nm, irradiates the sample. The change in signal induced by the T-jump (transmission for IR or back-emitted fluorescence light) is detected in real-time; hence, a very accurate baseline is automatically provided, and quite small changes can be determined. In both cases, the wavelength of the pump pulse corresponds to the peak of a weak D_2O near-IR absorption band ($\varepsilon = 10.1$ cm^{-1} at 2 μm) and was chosen because 80% of the light is transmitted through the 100-μm pathlength cells used in the studies. The high transmission ensures a nearly uniform temperature profile in the ~9 nL (300 μm × 300 μm × 100 μm)

laser interaction volume. The cells are identical for both the IR and fluorescence studies; they consist of sandwiched CaF_2 windows separated by a 100-μm spacer that is split into two separate compartments. The laser energy is absorbed by water (D_2O), and the temperature of the volume of water reaches its maximum value within ~20 ns (twice the FWHM of the pump pulse), since its temperature thermalization and diffusion within water occur on subnanosecond time scales. The diffusion of heat out of the interaction volume takes ~20 ms in our cells.

The pump pulse and IR production used for the IR studies has been previously described (Williams et al., 1996; Gilmanshin et al., 1997). This spectrometer consists of a widely tunable (from 1600 to 1700 cm^{-1}) CW lead salt infrared diode laser (Laser Analytics, Laser Components Instrument Group, Wilmington, MA) that functions as the probe for the IR measurements. An injection-seeded, Q-switched GCR-4 Nd:YAG laser (Spectra Physics, Mountainview, CA) and Raman shifter (one Stokes shift in H_2 gas) produce the pump radiation at 2 μm (10-ns FWHM Gaussian pulse width) that is the source for the temperature jump. The net instrument response time (a convolution of the heating and detector response times) is ~23 ns. The size of the T-jump was calibrated using the change in D_2O absorbance with temperature which acts as an internal thermometer in the range of 1632–1700 cm^{-1} (Williams et al., 1996). The T-jump was determined to within 2°C.

The temperature jump spectrometer used for the fluorescence studies has also been previously described (Gulotta et al., 2001). The pump pulse used for the fluorescence studies employs a Spectra Physics GCR-4 Nd:YAG laser (Spectra Physics, Mountainview, CA) operating at 1.06 μm pumping a six-foot Raman shifter filled with hydrogen gas (200 psi) to generate 20 mJ of 1.9 μm light. The 275-nm light is produced by a Spectra Physics argon ion laser (model 2045). The UV probe laser beam was focused to ~25 μm in the sample with the IR pump pulse focused to 500 μm. This apparatus is capable of delivering enough light to create a 40–50°C temperature jump; however, jumps were limited to <20°C since randomly occurring sample cavitations were produced in the sample at higher-magnitude T-jumps (Wray et al., 2002). A tryptophan solution was used to measure the magnitude of the temperature jump. The change in Trp fluorescence induced by the T-jump in the Trp reference solution was compared to static measurements, and this served to calibrate the size of the T-jump (accuracy, 1°C).

RESULTS

The amide-I′ absorption bands of apoMb-E at 20 (*solid line*) and at 58°C (*long dashed line*) are presented in Fig. 2 *a*. The second derivatives of both spectra which overlay the absorption spectra show multicomponent bands centered near 1648 cm^{-1}. Fourier self-deconvolution shows similar bands (data not shown). We assign this band to buried α-helices. The broadness of the peak is due to the variety of H-bonding partners and dipole-dipole couplings encountered (Surewicz and Mantsch, 1988). In addition, there is a smaller negative lobe in the second derivative spectrum at 1675 cm^{-1}. A less intense band at 1668–1675 cm^{-1} is generally observed for unfolded proteins and peptides and assigned to solvent-exposed disordered structure (Chirgadze et al., 1973; Jackson and Mantsch, 1991, 1995; Gilmanshin et al., 1996, 2001; Williams et al., 1996). According to the literature, the amide-I′ absorption of α-helices formed by peptides or destabilized proteins is shifted to lower frequencies (1630–1645 cm^{-1}) compared to the frequency of α-helices found in native proteins (Chirgadze and Brazhnikov, 1974; Haris and Chapman, 1995; Martinez and Millhauser, 1995; Reisdorf and Krimm, 1996; Williams et al., 1996). This ''red'' shift is attributed to a greater exposure of the helix backbone to water (Haris and Chapman, 1995; Reisdorf and Krimm, 1996; Gilmanshin et al., 1997; Manas et al., 2000), hence the label ''solvated'' helix. Recently, isotope-edited FTIR measurements on a coiled-coil peptide fragment of GCN4 convincingly demonstrated the assignment of the solvated portion of the coiled coil to a low helix frequency (1632 cm^{-1}); in contrast, the buried helix frequency (1648 cm^{-1}) is observed for residues in the interior of the coiled-coil (Manas et al., 2000). A weak shoulder at ~1634 cm^{-1} is seen in the second derivative spectrum at 20°C indicating the presence of a small amount of solvated helix in the E-form of sperm whale apomyoglobin. This shoulder disappears at higher temperatures. Fig. 2 *b* shows the difference FTIR spectra of E-form sperm whale apomyoglobin generated by subtracting the spectrum at 11.2°C from the spectra at higher temperatures. The figure verifies the existence of some temperature-dependent IR signal near 1633 cm^{-1} in the spectrum of E. It also shows that the decrease in the 1633 cm^{-1} band is accompanied by an increase at 1667 cm^{-1}. Structurally, the difference spectra indicate that solvent-exposed α-helices melt into disordered solvent-exposed polypeptides.

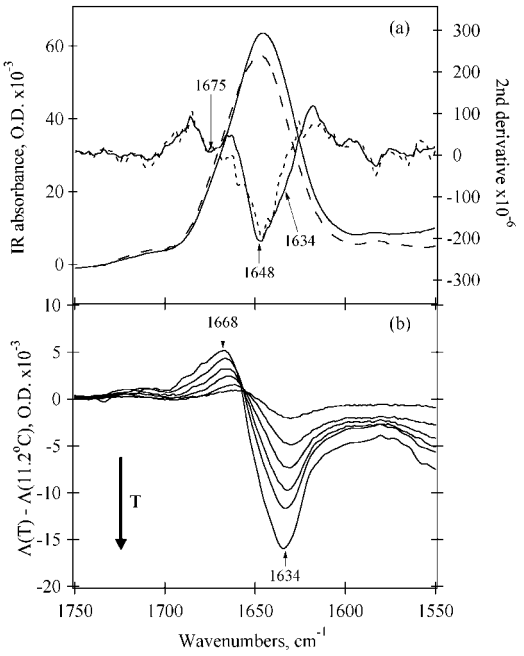

FIGURE 2 IR absorbance data for sperm whale apomyoglobin at pH* 3.0, 30 mM NaCl (*a*) amide-I spectra at 20.2°C (*solid line*), and 58.4°C (*long dashed line*); bold solid and short dashed lines are the second derivatives of the amide-I′ spectra taken at 20.2 and 58.4°C, respectively. (*b*) Difference spectra; the spectrum at 11.2°C has been subtracted from the spectrum at higher temperatures: 20.2°C, 30.2°C, 39.5°C, 48.9°C, 58.4°C, and 77.0°C.

The temperature-dependence of three key amide-I′ bands is shown in Fig. 3 *c*. The shape of the melting curve using the intensity of IR absorbance at 1648 cm^{-1}, a frequency close to the maximum position of the absorbance of α-helical

secondary structure in proteins, shows a somewhat different temperature-dependence than that found in the CD or fluorescence study (Fig. 3; discussed below). A reliable value for the T_M of the sigmoidal-like melting shown at 1648 cm^{-1} between 30–80°C could not be determined insamuch as the transition is very wide and may not yet have leveled out at the highest temperature measurable in these experiments. The amide-I component at 1633 cm^{-1} yields a melting transition that is essentially linear with a steep slope. The absorbance at this frequency is dominated by solvated helices; hence, the extent of their melting is approximately the same throughout the whole temperature range measured. The transition measured at 1668 cm^{-1} is of somewhat more complex character. A sigmoidal-like transition between 30–80°C is observed at this frequency, superimposed on a monotonic increase in intensity. This observation is consistent with the melting of both helical types, solvated and buried native-like, to produce disordered solvent-exposed polypeptide which is typically observed near 1668 cm^{-1}. Thus, the growth of the disordered structure band at 1668 cm^{-1} is correlated with the melting behavior of both types of helix. The temperature-dependent trends in the infrared data shown in Fig. 3 *c* are in close agreement to those shown for the horse heart protein (Williams et al., 1996; Gilmanshin et al., 1997, 2001).

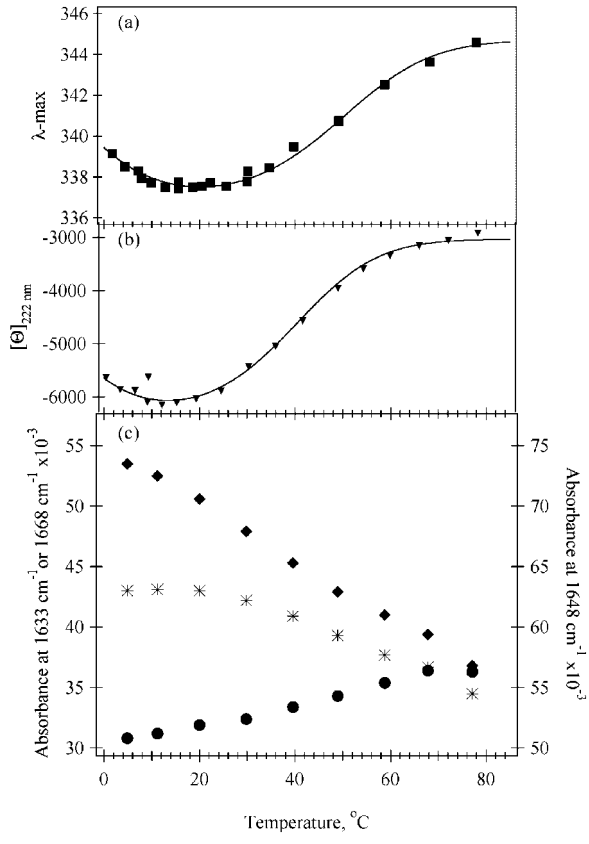

FIGURE 3 Temperature-dependencies of spectral parameters of sperm whale apomyoglobin at pH* 3.0, 20 mM NaCl. (*a*) Fluorescence emission maximum position (λ_{max}). (*b*) molar ellipticity at 222 nm ($[\Theta]_{222nm}$). (*c*) IR melting transitions at key wavenumbers: 1633 cm^{-1} (♦), 1648 cm^{-1} (*), 1668 cm^{-1} (●). The solid curve in *a* and *b* is the van't Hoff analysis fit to the E-form data, taking into account a finite heat capacity change between the folded and unfolded structures (see text).

The fluorescence data of Fig. 3 *a* exhibit a sigmoidal transition for the melting of E-form sperm whale apomyoglobin. The high temperature value for the emission λ_{max} is at the same wavelength as that observed for an indole ring free in solution; hence, the AGH core has completely melted. The beginning of cold denaturation is clearly evident in the data; hence, ΔC_p, the difference in heat capacity between the folded and unfolded states, must be introduced to analyze the data (compare with Fersht, 1999). The solid line plotted on top of the data is a van't Hoff analysis using the functional form, $\Delta G(T) = \Delta H(T) + \Delta C_p \times (T - T_m) - T \times (\Delta H(T)/T_m) + \Delta C_p \times \ln(T/T_m)$ to fit the data (Fersht, 1999), taking into account the finite heat capacity change between the folded and unfolded structures: $\Delta H = 12.5\ (\pm 2)$ kcal/mol, $\Delta C_p = 575\ (\pm 35)$ cal $\times$ mol^{-1} $\times$ deg^{-1}, and $T_m = 42\ (\pm 2)$ °C. The margin of error is estimated so that the van't Hoff function fits the entire high temperature melting profile. Notice, the derived T_m is somewhat lower than what would be expected from looking at the curve. In fitting the data of Fig. 3 *a*, it is clear that there is substantial overlap between hot and cold denaturation transitions; the melting transition is only 70–80% completed at the minimum shown on the graph which makes the apparent T_m appear higher. Using the same procedure to analyze melting transition for E-form sperm whale apomyoglobin as monitored by the change in molar ellipticity at 222 nm (Fig. 3 *b*) yields: $\Delta H = 12\ (\pm 2)$ kcal/mol, $\Delta C_p = 650\ (\pm 50)$ cal $\times$ mol^{-1} $\times$ deg^{-1}, and $T_m = 32\ (\pm 1)$°C.

It is clear that the change in heat capacity as E unfolds is quite large. The actual value obtained from the van't Hoff analyses depends on the spectroscopic probe used to measure the transition. Since Trp emission likely more accurately monitors just core formation, the ΔC_p from Trp emission is likely more accurate. However, either value suggests that a large number of hydrophobic residues are exposed to solvent in the transition since this is the main effect in determining the size of ΔC_p (Makhatadze and Privalov, 1990). Using a rough average value of ΔC_p of unfolding of ~22 cal/deg $\times$ mol per residue as is appropriate for apomyoglobin (Privalov and Makhatadze, 1990), ~26–30 residues take part in the melting.

The relaxation kinetics of the E-state were probed near the midpoint of the melting transition. Jumps to higher temperatures in this region shift the equilibrium toward a more unfolded distribution. Fig. 4 shows the frequency-dependence for temperature jumps between 46 and 53°C. A bleach is observed at frequencies due to the helical bands (solvated and buried helix, 1635 and 1648 cm^{-1}, respectively). A transient absorbance is observed at a frequency corresponding to the disordered structure band centered near 1668 cm^{-1}.

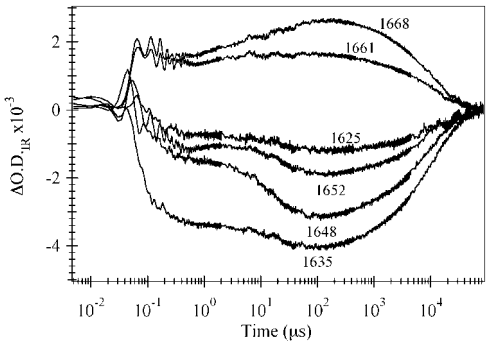

FIGURE 4 IR kinetics traces for the E-state of sperm whale apomyoglobin at pH* 3.0, 30 mM NaCl after a T-jump from 46 to 53°C. The wavenumber monitored during the transition is given in the diagram.

The decrease in 1635 and 1648 cm^{-1} bands and the concomitant appearance of intensity in the 1668 cm^{-1} band is consistent with the T-jump causing a shift in the equilibrium toward the unfolded state. Two major kinetics phases are observed at all frequencies, but the ratio of the amplitudes of the two phases is strongly wavelength-dependent. Fig. 5 compares the frequency-dependent magnitude of the transient IR absorption to the FTIR difference spectrum between 49 and 54°C. The static difference infrared spectrum (*solid line*) follows the shape and amplitude of the transient absorbance change over 200 μs indicating that the structural change seen in the steady-state IR data is over within 200 μs. There are two phases in the kinetic transients that occur within 200 μs. There is a substantial early phase, complete in 350 ns (τ = 55 ns), in the T-jump transients which is comparable to what is observed for horse heart apoMb and many small peptides (Gilmanshin et al., 1997). Fig. 5 shows that this phase is centered near the 1634 cm^{-1} band, indicating that it is due to the fast melting of solvated helices throughout the protein. The slow phase alone is represented by the difference between the 200-μs and the 350-ns times and exhibits a very different frequency-dependence than the fast phase. For this phase there is a dominant negative lobe near 1648 cm^{-1} and a positive lobe above 1668 cm^{-1}. We attribute this second phase to the melting of native α-helices and the resulting formation of disordered structure, a result consistent with previously described static data.

The relaxation kinetics of the formation of U from E after a laser T-jump were probed by tryptophan fluorescence intensity and IR absorbance at the amide-I′ frequency for the buried helix (1648 cm^{-1}) in a series of similar-magnitude temperature jumps to achieve various final temperatures. Fig. 6 shows the results for a temperature jump from 39 to 46°C probed by IR absorbance and from 35 to 52°C probed by fluorescence emission. Single exponential kinetics are observed in the fluorescence data both for this jump and for all other jumps tried. The emission results show a weakly temperature-dependent (Fig. 7) lifetime of 20 μs at this final temperature of 52°C. The infrared T-jump spectrum shown is clearly not single exponential but is well fit to a double exponential with τ_1 = 5 μs and τ_2 = 56 μs. However, infrared T-jumps to higher temperatures fit just as well to either a double or a single exponential function. An Arrhenius plot of the data is shown in Fig. 7. From a physical standpoint, it is very unlikely that a process taking place at low temperature simply ceases to exist as the temperature is increased. Much more likely is that the two processes have similar times and hence are not well resolved in our data sets. Therefore, we assumed double exponential behavior for all of the IR T-jump measurements. We also assumed that the

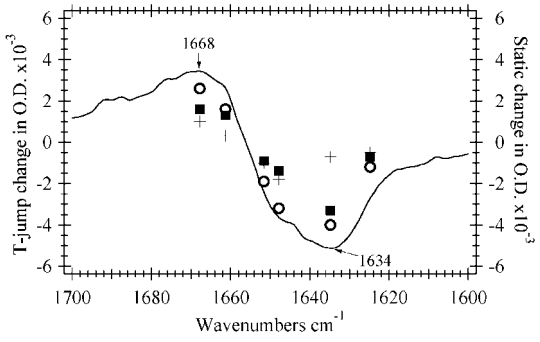

FIGURE 5 Comparison between the steady-state changes in IR absorbance upon going from 48.9°C to 53.7°C (*solid line*) and the transient absorbance change over the first 350 ns (ΔA_{350ns}, ■), 200 μs ($\Delta A_{200\mu s}$, ○), or between 350 ns and 200 μs ($\Delta A_{200\mu s} - \Delta A_{350ns}$, +) during a temperature jump between 46 and 53°C. The concentration of apomyoglobin in sample used for the steady-state data was 3 mg/ml whereas that used for the temperature jump measurements was 6 mg/ml. The steady-state measurements were done using a 56-μm pathlength spacer and the spacer used for the temperature-jump measurements was 100 μm. The steady-state curve has been multiplied by suitable factors to account for the concentration and pathlength differences and the difference in temperature range.

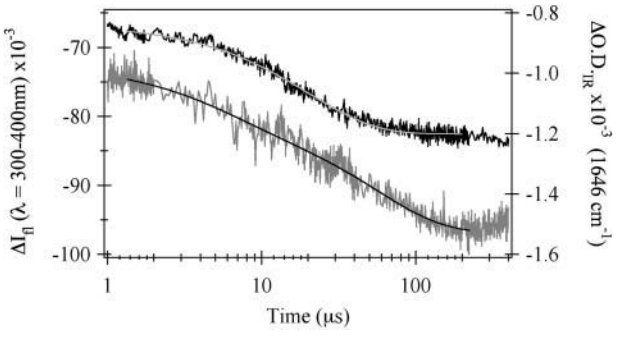

FIGURE 6 Fluorescence (*black*) and IR (*gray*) kinetics traces for the E-form of sperm whale apomyoglobin. The concentration of apomyoglobin in the fluorescence sample was 3.3 mg/ml in pH* 3.0 15 mM NaCl solution and the jump was from 35°C to 52°C. The data is well fit to a single exponential with τ = 20 μs (*gray line*). For the IR sample, the concentration of apomyoglobin was 4 mg/ml in pH* 3.0 30 mM NaCl. IR changes were monitored at 1648 cm^{-1} during a jump from 39 to 46°C. The data cannot be fit with a single exponential but is well fit by a double exponential with τ_1 = 5 μs and τ_2 = 56 μs (*black line*).

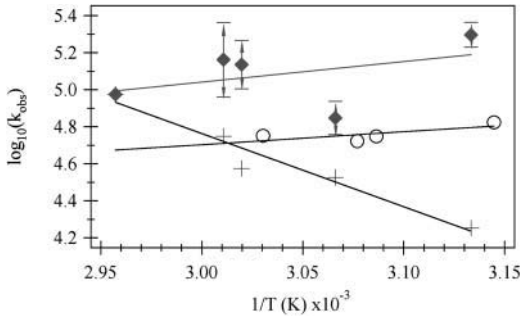

FIGURE 7 Arrhenius plot showing the temperature dependence of the phases. The values of T used for the $(1/T)$ axis are the final temperatures reached during the jump. k_{obs} is the value obtained from a single exponential fit of the fluorescence (o) or a constrained double exponential fit of the infrared (+, ♦) T-jump data. The 46°C data was fit to a unconstrained double exponential. Then the ratio of the two phases found for the 46°C data was used to constrain the double exponential fit for the other curves. The error bars on the fast phase of the IR data were determined by taking the standard deviation of the rate constants from several constrained and unconstrained double exponential fits to the data and then adding or subtracting this number from the value of the datapoint.

relative change in the IR absorbance caused by each process is the same regardless of jump temperature and held the ratio of the two processes to the values obtained from a free double exponential fit of the 46°C data. The values for k_{obs} for the IR T-jump data, shown in Fig. 7, are the results of the constrained double exponential fit. $Log_{10}(k_{obs})$ for the fast phase slightly decreases as the final temperature is increased whereas the $\log_{10}(k_{obs})$ for the slow phase strongly increases. The rates of the two phases become closer together as the temperature is increased and are completely indistinguishable at 65°C. The weakly-decreasing $\log_{10}(k_{obs})$ versus $1/T$ data for the fluorescence phase intersects the more strongly temperature-dependent slow phase seen in the infrared T-jump data at ~57°C.

Table 1 compares the thermodynamic values obtained from fluorescence and CD studies on the sperm whale protein with those found for the horse heart protein at pH* 3.0, 20 mM NaCl (Gilmanshin et al., 1997, 2001). Substantially lower values for ΔH and ΔC_p are found for the sperm whale protein because the melting transition is much less steep. This indicates that fewer residues are involved in the core for E-form sperm whale apomyoglobin relative to the horse heart conformation. Another possibility is that core formation involves burial of less surface area, due to the differences in sequence in this region of the protein as an alternative or additional cause of our results. However, comparison of the sequences make this unlikely. Out of the 40 residues within and next to the core region, seven are different between sperm whale and horse heart sequences, but in only two cases does the difference arise from different hydrophobicity designations (Privalov and Makhatadze, 1990). The melting temperature from the fluorescence melting study is somewhat lower for the sperm whale

TABLE 1 Thermodynamic parameters

	Horse heart*		Sperm whale	
	Fluorescence	CD	Fluorescence	CD
ΔH	21	26	12.5	12
ΔS	65	83	40	39
ΔC_p	750	950	575	650
T_m	48	43	42	32

The thermodynamic parameters relevant for the formation of the E-form of horse heart and sperm whale apomyoglobins with ΔH (kcal/mol), ΔS (cal/deg × mol), ΔC_p (cal/deg × mol), and T_m (°C).
*Taken from Gilmanshin et al. (2001).

protein than the horse heart protein. The discrepancy in the melting temperatures found from the CD data is much larger indicating a greater heterogeneity in the E-forms of sperm whale apomyoglobin. This also supports the conclusion that there are fewer residues in the core.

DISCUSSION

Several spectroscopic probes were used to characterize the dynamical nature of sperm whale E. Each has its own strengths depending on what structural attribute is being probed. There are two Trp residues in sperm whale apomyoglobin located in the A-helix (Trp7 and Trp14). The indole rings of these Trp residues are known to be partly buried in the A-G-H core of the native protein, and their fluorescence properties are affected by solvent exposure. Thus, Trp fluorescence has been used as a monitor of the presence of the A-G-H core. The molar ellipticity at 222 nm is the characteristic wavelength employed for monitoring overall helical content, which is particularly useful for this largely α-helical protein. The infrared spectrum in the amide-I′ region contains ''marker bands'' indicative of helices buried in a hydrophobic environment like the core (marker frequency near 1650 cm^{-1}), helices which are solvated (1630–1640 cm^{-1}), and solvated disordered structures (near 1665 cm^{-1}). Both CD and IR techniques report on global secondary structure content, but IR absorption is also influenced by the formation of specific tertiary structures, such as helix-helix packing which excludes solvent.

Structure of E

We previously performed a similar spectroscopic and kinetic study of the E-state of horse heart apomyoglobin (Gilmanshin et al., 1998, 2001; Gulotta et al., 2001). The present report shows that the two proteins have very similar spectroscopic properties. As in the case of the horse heart protein, it is clear from the evidence presented here that a highly destabilized acid form of sperm whale apomyoglobin exists at pH* 3.0 (low salt) but that the protein still retains tertiary structure. Melting curves constructed from CD, Trp emission, and IR absorption show a nonlinear shape indicative of

cooperative melting behavior. From the changes in emission of the indole ring(s) of Trps 7 and 14 as E melts, that show a transformation from partially buried to completely exposed indole rings, the present measurements suggest that a portion of the A-helix participates in the tertiary structure of E. From the measured size of the change in heat capacity as E melts, it can be estimated that ~26–30 residues take part in the melting (see Results). This is similar to that found in the horse heart protein (34–43 residues), but distinctly a smaller number. From recent NMR measurements of the I-form of sperm whale apoMb that show the A-G-H core intact (Eliezer et al., 1998; Eliezer et al., 2000) and that portions of the A-helix are involved in the tertiary structure of E (as revealed from the present results of the Trp emission), it seems certain that the tertiary structure of the more acid-destabilized E also consists of the association of a portion of the A-helix with the central portion of G through H.

Like its horse heart counterpart, the data favor a structural model wherein sperm whale E consists of multiple conformations, each of which retains some portion of the A-G-H core. There are several reasons for this view. Although it is clear that E undergoes a sigmoidal high-temperature melt (at least for Trp emission and CD), the shape of the melting transition that is observed varies depending on the spectroscopic technique employed (CD, Trp emission, IR) and, hence, the specific structural attribute which is probed. This is typically taken as evidence for a sequential melting transition. Here, the melting curves overlap substantially so that the various states must be quite close in energy and, hence, simultaneously present at lower temperatures. This is consistent also with the small number of residues within the folded portion of E. On physical grounds, it would be difficult to find a unique structural arrangement substantially lower in energy than others with so few residues taking part. Lastly and importantly, the kinetics results from the temperature-jump studies show multiple different relaxation times (5–60 μs), which are best described by a collapse of U to distinct E-forms via a parallel folding kinetics model (see below).

Stability of sperm whale versus horse heart ApoMb

It is well known that the native structures of sperm whale myoglobin and apoMb are substantially more stable than other myoglobins and their apo-proteins. Using experimental data from normalized fluorescence or CD intensity versus [Guanidine HCl] and applying a three-state model based on the one proposed by Barrick and Baldwin (1993) and Barrick et al. (1994), Scott and co-workers found that the unfolding of horse heart N is more facile then the sperm whale protein since the overall unfolding equilibrium constant for sperm whale apomyoglobin is smaller than that of the horse heart apoprotein by a factor of 67 (Scott et al., 2000). It therefore comes as a surprise at first that the enthalpy of forming the core of the E-form of the sperm whale protein is substantially smaller than horse heart E (Table 1). It has been shown, however, that there is no single or small group of particular residues which are responsible for this difference in stability in the native proteins, and, moreover, many of the residues which are known to be involved in making up the differential stabilities of myoglobins lie outside of the core region. This is supported by Scott and co-workers' finding that the sperm whale unfolding constant for the I $\leftrightarrow$ U transition was only a factor-of-6 smaller than that of the horse heart species (Scott et al., 2000). Hence, our results suggest that the stability of the first forming structure when a polypeptide collapses need not be an indicator of that for the final folded protein.

Kinetics

The temperature-jump experiments perturb the equilibrium between E and its temperature-unfolded state, U. Consequently, it is the kinetics of this transition that are measured. The structure of the temperature-unfolded E may or may not be identical to the acid-unfolded (U state) that has been well characterized recently by NMR (Eliezer et al., 1998; Yao et al., 2001)]. In this latter U-form, there is no evidence of tertiary structure, and this is likely also true of temperature-melted E since, at high temperature, the Trp residues are completely solvent-exposed (indicating the absence of A-G-H core). Moreover, there are only small amounts of residual secondary structure as judged from the small signals at 222 nm in the CD measurements (Fig. 3 *b*). The acid-unfolded state is found to contain some small amounts of secondary structure (a portion of the H-helix, some of the G-H turn, and a section of helices D–E retain some helical formation; Shin et al., 1993; Eliezer et al., 1998), and this may also be true for the melted E.

The overall pattern of the kinetics results of the sperm whale E is quite similar, but not identical, to that found for the E-form of horse heart (Gilmanshin et al., 1997; Gulotta et al., 2001). A submicrosecond phase is observed at 55 ns (Fig. 4) for the sperm whale protein versus 35 ns for horse heart (Gilmanshin et al., 1998). This is close to the relaxation times associated with the melting of loosely or nonpacked solvated helices (Callender et al., 1998; Dyer et al., 1998), and the transient observed at 55 ns occurs near a ''marker'' position (1634 cm^{-1}) in the IR spectrum associated with solvated helices (Fig. 5). It would seem that the melting associated with the 55-ns relaxation time occurs in regions of the protein probably not associated with the formation of tertiary structure.

Three relaxation times are observed on the microsecond time scale, and all three involve the formation of tertiary structure (A-G-H ''core'' following the arguments of the structure of E above). A single fast relaxation phase, 20 μs at 52°C, is observed for all measurements of the kinetic changes in Trp emission, which indicates core formation

(burial of a Trp indole ring). This 20-μs transient is very weakly temperature-dependent. The infrared kinetics data, taken at 1648 cm^{-1}, close to the marker band position for collapsed desolvated helix, requires two exponentials for a good fit to at least one of the data sets (see Results), a ''slow'' phase (56 μs at 46°C) and a ''fast'' phase (5 μs at 46°C). The slow phase is highly temperature-dependent with apparent energy of activation of 18 kcal/mole, indicative of a process with a strong enthalpic barrier. The fast time observed in the IR kinetics (like the emission data) is very weakly temperature-dependent, indicative of a low enthalpic barrier. For comparison, like the sperm whale protein, the fluorescence T-jump data are monoexponential, weakly temperature-dependent and fast in the horse heart system (Gulotta et al., 2001). The IR T-jump data for both proteins show double exponential behavior and include a slow time not seen via fluorescence and which shows a substantial temperature dependence. The central difference between the kinetic response of the two proteins is that the fast relaxation time in the sperm whale protein found in the IR is clearly at a different value than that derived from the fluorescence kinetics whereas, in the horse heart system, the two are the same.

Kinetic model

The existence of three times in the relaxation kinetics for sperm whale requires a minimum of four states. We assume that the unfolded U-form is, for the purposes of a kinetics model, a single species (i.e., rapidly interconverting). Hence, any kinetics model requires three folded states containing tertiary structure, E_1, E_2, and E_3. It is not necessary, of course, that all three E-forms be significantly populated at equilibrium; one or more of these may be an intermediate between E and U that is significantly populated transiently after melting is initiated. Our kinetics experiments are all done starting with the protein in the E-form and then the protein is unfolded by rapid heating produced in the T-jump so the kinetic models must be in accord with this direction of the process. Hence, to be observed, the fast phases must precede the slow phase as E melts to form U. With the exception of the second time seen in the infrared data not being the same as the fluorescence relaxation rate, the temperature-jump data for the sperm whale system is very similar to that seen for the horse heart protein and the development of a kinetics model follows the same lines as the one we previously outlined, in detail, for the horse heart protein (Gulotta et al., 2001). We found there that, given the putative structures of E and U, the observed kinetics on the microsecond time scale are not well described by a strictly sequential model of interconversions of the four species. In brief, the absence of any ''slow'' phase kinetics in the fluorescence data means that there is no change in the concentration of species that modify Trp environment(s). It is very difficult to find conditions that yield a single exponential process for a single first fast step, found in the emission dynamics, whereas the IR dynamics are characterized by a biexponential process with constituents of approximately equal amplitude if a sequential model is used. In a sequential course of events, the E1 $\leftrightarrow$ E2 equilibrium would be established first but the ''slow'' event, formation of E3, would disrupt the ''fast'' equilibrium and, hence, would show up in the kinetics of the Trp emission. Therefore, it seems clear that modeling of the kinetic pathway from E to U involves the need to invoke parallel processes, and Scheme 1 or 2 are adequate to model the data. Our results cannot distinguish between these two models.

$$\begin{array}{c} E_1 \leftrightarrow E_2 \leftrightarrow U \\ \cdots \\ E_3 \leftrightarrow U \end{array} \qquad \begin{array}{c} E_1 \leftrightarrow U \\ \cdots \\ E_2 \leftrightarrow U \\ \cdots \\ E_3 \leftrightarrow U \end{array}$$

SCHEME 1 SCHEME 2

Physically, in either scheme, our results indicate that the rapid phase(s), 5 μs at 46°C in the IR and 20 μs at 52°C in the Trp emission, respectively, which are energetically favorable, involve the formation of collapsed native-like structures and are likely to be a diffusion-limited collapse of a subset of conformations of U that contains elements of secondary structure which resemble that found in the core and are close to a proper alignment. The timescale of the fast process, $\sim$10 μs, is on the order of the diffusion of the two ends of a protein loop the size of apomyoglobin to meet from a disordered state if the loop between the A and G-H portions of the apoMb structure is taken to be 80–100 residues (Flory, 1969; Szabo et al., 1980; Hagen and Eaton, 2000; Lapidus et al., 2000; Hagen et al., 2001). A similar rate has been observed for the collapse of a helix-forming peptide compared to a disordered glycine-containing peptide (Lapidus et al., 2000). The rate is also consistent with the specific diffusion-collision model of apomyoglobin folding (Pappu and Weaver, 1998). The formation of the A-G-H core on the timescale of the diffusion of the ends of the polypeptide chain together in an activationless process implies that the probability of such encounters producing a stable folded structure is very high. Successful formation of the core structure requires proper alignment of the sidechains to form the correct tertiary interactions (and to avoid nonnative interactions), which in turn requires the correct (i.e., helical) alignment of the backbone. The population of helix in H and the population of the proper G-H turn conformation are believed to be high (Shin et al., 1993; Waltho et al., 1993). However, the helix propensity of G in water, and hence its equilibrium concentration, is low and the helix propensity of A in water is uncertain (Reymond et al., 1997; Yao et al., 2001). Clearly, a high transient helix propensity for the A- and H-helices are needed to reconcile the fast formation

times observed here. This could be achieved through the partial removal of solvent water as the two ends of the molecule approach one another, as suggested previously with regards to helix formation in A (Reymond et al., 1997) and implicitly by the diffusion-collision model (Pappu and Weaver, 1998), but before any fixed tertiary interactions are established.

The relatively ''slow'' phase (56 μs at 46°C), conversely, is an activated process and involves an energy barrier between U and folded E. It seems likely this process involves subsets of unfolded populations that are either less well aligned or a folded state that is less nativelike. Collapse of encounter complexes then requires rearrangement over a barrier to arrive at a stable structure.

This general picture of the folding dynamics, qualitatively the same as found for the horse heart protein (Gulotta et al., 2001), is consistent with the heterogeneous nature of E; various sub-states fold along different pathways. This seems advantageous since it is more efficient to condense into a compact core-like structure if there are multiple ways in which stable tertiary contacts can be made.

This work was supported by the National Science Foundation, MCB-9727439 (R.H.C.), and the Institute of General Medicine, National Institutes of Health GM53640 (R.B.D.) and GM35183 (R.H.C.).

REFERENCES

Barrick, D., and R. L. Baldwin. 1993. The molten globule intermediate of apomyoglobin and the process of protein folding. *Prot. Sci.* 2:869–876.

Barrick, D., F. Hughson, and R. Baldwin. 1994. Molecular mechanisms of acid denaturation The role of histidine residues in the partial unfolding of apomyoglobin. *J. Mol. Biol.* 237:588–601.

Callender, R., R. Gilmanshin, R. B. Dyer, and W. Woodruff. 1998. The primary processes of protein folding. *Annu. Rev. of Phys. Chem.* 49:173–202.

Chirgadze, Y. N., and E. V. Brazhnikov. 1974. Intensities and other spectral parameters of infrared amide bands of polypeptides in the alpha-helical form. *Biopolymers.* 13:1701–1712.

Chirgadze, Y. N., B. V. Shestopalov, and S. Y. Venyaminov. 1973. Intensities and other spectral parameters of infrared amide bands of polypeptides in the β- and random forms. *Biopolymers.* 12:1337–1351.

Crumpton, M. J., and A. Polson. 1965. A comparison of the conformation of sperm whale metmyoglobin with that of apomyoglobin. *J. Mol. Biol.* 11:722–729.

Dyer, R. B., F. Gai, W. Woodruff, R. Gilmanshin, and R. H. Callender. 1998. Infrared studies of fast events in protein folding. *Acc. Chem. Res.* 31:709–716.

Dyson, H. J., and P. E. Wright. 1998. Equilibrium NMR studies of unfolded and partially folded proteins. *Nat. Struc. Biol. NMR Suppl.* 5:499–503.

Eliezer, D., J. Chung, H. J. Dyson, and P. E. Wright. 2000. Native and non-native secondary structure and dynamics in the pH 4 intermediate of apomyoglobin. *Biochemistry.* 39:2894–2901.

Eliezer, D., and P. E. Wright. 1996. Is apomyoglobin a molten globule? Structural characterization by NMR. *J. Mol. Biol.* 263:531–538.

Eliezer, D., J. Yao, H. J. Dyson, and P. E. Wright. 1998. Structural and dynamic characterization of partially folded states of apomyoglobin and implications for protein folding. *Nat. Struct. Biol.* 5:148–155.

Fersht, A. 1999. Structure and Mechanism in Protein Science: A Guide to Enzyme Catalysis and Protein Folding. Freeman and Company, New York.

Flory, P. 1969. Statistical Mechanics of Chain Molecules. John Wiley, New York.

Gilmanshin, R., R. H. Callender, and R. B. Dyer. 1998. The core of apomyoglobin folds at the diffusion limit. *Nat. Struct. Biol.* 5:363–365.

Gilmanshin, R., R. B. Dyer, and R. H. Callender. 1997. Structural heterogeneity of the various forms of apomyoglobin: implications for protein folding. *Prot. Sci.* 6:2134–2142.

Gilmanshin, R., M. Gulotta, R. B. Dyer, and R. H. Callender. 2001. Structures of apomyoglobin's various acid-destabilized forms. *Biochemistry.* 40:5127–5136.

Gilmanshin, R., J. Van Beek, and R. Callender. 1996. Study of the ribonuclease S-peptide/S-protein complex by means of Raman difference spectroscopy. *J. Phys. Chem.* 100:16754–16760.

Gilmanshin, R., S. Williams, R. H. Callender, R. B. Dyer, and W. H. Woodruff. 1997. Fast events in protein folding: relaxation dynamics and structure of the I-form of apomyoglobin. *Biochemistry.* 36:15006–15012.

Gilmanshin, R., S. Williams, R. H. Callender, W. Woodruff, and R. B. Dyer. 1997. Fast events in protein folding: relaxation dynamics of secondary and tertiary structure in native apomyoglobin. *Proc. Natl. Acad. Sci. USA.* 94:3709–3713.

Griko, Y. V., and P. L. Privalov. 1994. Thermodynamic puzzle of apomyoglobin unfolding. *J. Mol. Biol.* 235:1318–1325.

Griko, Y. V., P. L. Privalov, S. Y. Venyaminov, and V. P. Kutyshenko. 1988. Thermodynamic study of the apomyoglobin structure. *J. Mol. Biol.* 202:127–138.

Gulotta, M., R. Gilmanshin, R. H. Callender, and R. B. Dyer. 2001. Core formation in apomyoglobin: probing the upper reaches of the folding energy landscape. *Biochemistry.* 40:5137–5143.

Hagen, S., C. Carswell, and E. Sjolander. 2001. Rate of interchain contact formation in an unfolded protein: temperature and denaturant effects. *J. Mol. Biol.* 305:1161–1171.

Hagen, S., and W. Eaton. 2000. Two-state expansion and collapse of a polypeptide. *J. Mol. Biol.* 301:1019–1027.

Haris, P. I., and D. Chapman. 1995. The conformational analysis of peptides using Fourier transform IR spectroscopy. *Biopolymers.* 37: 251–263.

Hughson, F. M., P. E. Wright, and R. L. Baldwin. 1990. Structural characterization of a partly folded apomyoglobin intermediate. *Science.* 249:1544–1548.

Jackson, M., and H. H. Mantsch. 1991. Beware of proteins in DMSO. *Biochim. Biophys. Acta.* 1078:231–235.

Jackson, M., and H. H. Mantsch. 1995. The use and misuse of FTIR spectroscopy in the determination of protein structure. *Crit. Rev. Biochem. Mol. Biol.* 30:95–120.

Jamin, M., and R. Baldwin. 1998. Two forms of the pH 4 folding intermediate of apomyoglobin. *J. Mol. Biol.* 276:491–504.

Lapidus, L., W. Eaton, and J. Hofrichter. 2000. Measuring the rate of intramolecular contact formation in polypeptides. *Proc. Natl. Acad. Sci. USA.* 97:7220–7225.

Lecomte, J. T., Y. H. Kao, and M. J. Cocco. 1996. The native state of apomyoglobin described by proton NMR spectroscopy: the A-B-G-H interface of wild-type sperm whale apomyoglobin. *Proteins.* 25: 267–285.

Loh, S. N., M. S. Kay, and R. L. Baldwin. 1995. Structure and stability of a second molten globule intermediate in the apomyoglobin folding pathway. *Proc. Natl. Acad. Sci. USA.* 92:5446–5450.

Makhatadze, G. I., and P. L. Privalov. 1990. Heat capacity of proteins. I. Partial molar heat capacity of individual amino acid residues in aqueous solution: hydration effect. *J. Mol. Biol.* 213:375–384.

Manas, E. S., Z. Getahun, W. W. Wright, W. F. DeGrado, and J. M. Vanderkooi. 2000. Infrared spectra of amide groups in α-helical proteins:

evidence for hydrogen bonding between helices and water. *J. Am. Chem. Soc.* 122:9883–9890.

Martinez, G., and G. Millhauser. 1995. FTIR spectroscopy of alanine-based peptides: assignment of the amide I′ modes for random coil and helix. *J. Struct. Biol.* 114:23–27.

Pappu, R. V., and D. L. Weaver. 1998. The early folding kinetics of apomyoglobin. *Prot. Sci.* 7:480–490.

Privalov, P. L., and G. I. Makhatadze. 1990. Heat capacity of proteins. II. Partial molar heat capacity of the unfolded polypeptide chain of proteins: protein unfolding effects. *J. Mol. Biol.* 213:385–391.

Reisdorf, W. C., Jr., and S. Krimm. 1996. Infrared amide I′ band of the coiled coil. *Biochemistry.* 35:1383–1386.

Reymond, M. T., G. Merutka, H. J. Dyson, and P. E. Wright. 1997. Folding propensities of peptide fragments of myoglobin. *Prot. Sci.* 6:706–716.

Scott, E. E., E. V. Paster, and J. S. Olson. 2000. The stabilities of mammalian apomyoglobins vary over a 600-fold range and can be enhanced by comparative mutagenesis. *J. Biol. Chem.* 275:27129–27136.

Shin, H.-C., G. Merutka, J. P. Waltho, L. L. Tennant, H. J. Dyson, and P. E. Wright. 1993. Peptide models of protein folding initiation sites. 3. The G-H helical hairpin of myoglobin. *Biochemistry.* 32:6356–6364.

Shin, H.-C., G. Merutka, J. P. Waltho, P. E. Wright, and H. J. Dyson. 1993. Peptide models of protein folding initiation sites. 2. The G-H turn region of myoglobin acts as a helix stop signal. *Biochemistry.* 32:6348–6355.

Springer, B. A., and S. G. Sligar. 1987. High-level expression of sperm whale myoglobin in *Escherichia coli. Proc. Natl. Acad. Sci. USA.* 84:8961–8965.

Surewicz, W. K., and H. H. Mantsch. 1988. New insight into protein secondary structure from resolution-enhanced infrared spectra. *Biochim. Biophys. Acta.* 952:115–130.

Szabo, A., K. Schulten, and Z. Schulten. 1980. First passage time approach to diffusion controlled reactions. *J. Chem. Phys.* 72:4350–4357.

Waltho, J. P., V. A. Feher, G. Merutka, H. J. Dyson, and P. E. Wright. 1993. Peptide models of protein folding initiation sites. 1. Secondary structure formation by peptides corresponding to the G-helix and H-helix of myoglobin. *Biochemistry.* 32:6337–6347.

Williams, S., T. P. Causgrove, R. Gilmanshin, K. S. Fang, W. H. Woodruff, R. H. Callender, and R. B. Dyer. 1996. Fast events in protein folding: Helix melting and formation in a small helical peptide. *Biochemistry.* 35:691–697.

Wray, W., T. Aida, and R. Dyer. 2002. Cavitation and heat transfer effects in laser-induced temperature-jump studies of protein dynamics. *Appl. Phys. B.* 74:55–66.

Yao, J., J. Chung, D. Eliezer, P. E. Wright, and H. J. Dyson. 2001. NMR structural and dynamic characterization of the acid-unfolded state of apomyoglobin provides insights into the early events in protein folding. *Biochemistry.* 40:3561–3571.